(This is a preprint of a paper published in Proc. SPIE Int. Symp. Medical Imaging 1998, San Diego, Feb 21-27, 1998
Ultrasonic Transducer Engineering Conference, edited by K. Shung)

Finite Element Modeling for Ultrasonic Transducers

Najib N. Abboud[a], Gregory L. Wojcik[b], David K. Vaughan[b],
John Mould[b], David J. Powell[b], Lisa Nikodym[b]

[a]Weidlinger Associates Inc., 375 Hudson Street, New York, NY 10014, USA
[b]Weidlinger Associates Inc., 4410 El Camino Real, Los Altos, CA 94022, USA

ABSTRACT

Finite element modeling is being adopted in the design of ultrasonic transducers and imaging arrays. Impetus is accelerated product design cycles and the need to push the technology. Existing designs are being optimized and new concepts are being explored. This recent acceptance follows the convergence of improvements on many fronts: necessary computer resources are more accessible, lean, specialized algorithms replacing general-purpose approaches, and better material characterization

The basics of the finite element method (FEM) for the coupled piezoelectric-acoustic problem are reviewed. We contrast different FEM formulations and discuss the implications of each: time-domain versus frequency domain, implicit versus explicit algorithms, linear versus nonlinear. Beyond discussions of the theoretical underpinnings of numerical methods, the paper also examines other modeling ingredients such as discretization, material attenuation, boundary conditions, farfield extrapolation, and electric circuits.

Particular emphasis is placed on material characterization, and this is discussed through an actual "model-build-test" validation sequence, undertaken recently. Some applications are also discussed.

Keywords: Arrays, Attenuation, Finite Element Method, Imaging, Piezoelectric, Transducer, Ultrasound

1. INTRODUCTION

Until recently, medical transducer designers relied almost exclusively on 1D analytical models and experimental prototypes. Now, many employ comprehensive finite element simulations for transient, 2D and 3D analyses. Effectiveness of their modeling is proportional to accuracy and completeness of material measurements, fidelity of geometrical and manufacturing process details, and the modeler's skill with numerical experiments and design strategies. Modeling skills rely on an intuitive understanding of the transducer's operational parameters and the overall design problem. This requires either years of experience or focused, practical training. Without such skills, modeling is often used poorly and results may be misinterpreted or erroneous, leading to wasted resources and market opportunities. As personal computers, modern finite element algorithms, and user interfaces make 2D/3D modeling more accessible, the required skill set needs to be taught quickly and efficiently to an eclectic mix of users.

Therefore, in our role as code developers, users, and trainers, we have sought a simple yet practical basis for teaching transducer fundamentals and the finite element modeling paradigm. The most direct basis would be closed-form solutions, but transducers generally have too many characteristic lengths for simple mathematical analysis. However, note that each segment of a typical medical transducer has a fairly short extensional resonance length, e.g., $\approx \lambda/2$ for the piezoceramic and $\approx \lambda/4$ for the matching layer(s). These fractional-wave dimensions suggest that relatively low frequency *coupled oscillators* rather than *propagating waves* can provide a simple, intuitive model of device physics. Although oscillator models cannot be quantitative, in general, they provide the simplest, complete representation of 1D electromechanical transducer behavior. This approach appears to have been passed over in the transducer literature and as a teaching aid. To this end, Section 2 examines simple spring-mass models that demonstrate basic device behavior and as well as introduce finite element fundamentals, given that springs and masses are the simplest "elements" of discrete numerical modeling.

[a] correspondence: Email: abboud@wai.com, Tel: (212) 367-3000, Web: www.wai.com
[b] correspondence: Email: flex_support@wai.com, Tel: (650) 949-3010, Web: www.wai.com

We then proceed in Section 3 to generalization of these electromechanical models, leading to the full 3D finite element formalism. This was first developed by Allik and Hughes in 1970 [1]. Although in use since then for analysis of low-frequency underwater projectors [2], its adoption in the medical ultrasound community remained limited until the early 1990's. The investigation of the then new 1-3 piezocomposites accentuated the need for such comprehensive modeling, as exemplified by the work of Hossack and Hayward [3]. The work of Lerch [4] emphasized the need for transient response modeling and non-uniform damping in realistic applications, features lacking in then available commercial software. It is the adoption of explicit wave propagation algorithms in PZFlex [5-11] however that made realistic transducer simulations practical. With demonstrated speed/size advantage factors of 100 over conventional implicit algorithms, broadband imaging transducer models became tractable on desktop computers. The point is that software used in a production capacity must rely on specialized algorithms rather than general-purpose ones. To this end, we contrast different FEM formulations and discuss the implications of each: time-domain versus frequency domain, implicit versus explicit algorithms, and linear versus nonlinear schemes.

Beyond discussions of the theoretical underpinnings of numerical methods, we examine in Section 4 modeling issues from the analyst's perspective: discretization, material dissipation, boundary conditions, farfield extrapolation, and electric circuits. The "quality" and "cost effectiveness" of the model depends on the proper use of these ingredients. We review their underlying assumptions and provide guidelines for optimal use.

Accuracy of the finite element model also hinges on accuracy of the material constitutive properties, and those provided in manufacturer specification sheets are often incomplete, if not inaccurate. Section 5 examines material characterization issues in the context of a recently undertaken validation exercise based on an incremental "model-build-test" analysis of a nonproprietary 1D biomedical imaging array. This sequence of component and device validations provides an excellent opportunity to identify characterization procedures that work and those that require further refinement, all while displaying its impact on the resultant finite element solution. Ultimately, validated and established characterization protocols are critical if numerical modeling is to serve as a "virtual prototyping" tool.

Some recent applications and studies are briefly discussed in Section 6, mainly to highlight some of the important points made earlier, to mention new ones that could not be discussed in detail in the body of the paper, and to provide some references to a broader range of applications.

2. COUPLED OSCILLATOR MODELS OF RESONANT TRANSDUCERS

Each segment of a typical medical transducer has a fairly short extensional resonance length, e.g., $\approx \lambda/2$ for the piezoceramic and $\approx \lambda/4$ for the matching layer(s). These fractional-wave dimensions suggest that relatively low frequency *coupled oscillators* rather than *propagating waves* can provide a simple, intuitive model of device physics. Although oscillator models cannot be quantitative, in general, they provide the simplest, complete representation of 1D electromechanical transducer behavior. As such, they are valuable in illustrating the "fundamentals".

To this end we examine what amounts to spring-mass models of transducer stack elements. These are the most fundamental electromechanical analogs and can be developed intuitively, as follows, or from more rigorous matrix structural analysis and finite element concepts. In particular, piezoelectric constitutive relations for the spring are derived from the continuum relations and applied to the simple harmonic oscillator. This is generalized to a coupled oscillator representing the lowest-order resonances in a piezoelectric transducer stack, i.e., backing, piezoelectric, matching layer(s), and water load.

2.1. Equations of motion and constitutive relations

The basis for approximate dynamic models, in general, is (1) assumption of a specific strain function, e.g., constant or linear, and (2) mass distribution, i.e., consistent or lumped. This is the foundation of matrix structural analysis [12], the predecessor of finite element methods. The strain function assumption yields ordinary differential equations in time by reducing the infinite degrees of freedom to a finite number, while the mass distribution assumption simplifies time integration.

Consider a 1D piezoelectric bar with length L and area A, electroded on the ends and poled lengthwise. Longitudinal displacement is $u(x,t)$, governed by the partial differential equation

$$\rho A \frac{\partial^2 u}{\partial t^2} = \frac{\partial T}{\partial x} \tag{2.1}$$

where x is the space coordinate, t is time, ρ is material density, and $T(x,t)$ is longitudinal stress. Boundary conditions are specified on u or T, along with initial conditions. The piezoelectric constitutive relations between stress T, strain $S = \partial u/\partial x$, electric field E, and electric displacement D are

$$T = c^E S - eE \quad , \quad D = \varepsilon^S E + eS \tag{2.2}$$

where c^E is elastic stiffness under constant electric field, e is the piezoelectric stress constant, and ε^S is electric permittivity under constant strain, e.g., see [13]. Because $\nabla \cdot D = 0$ (divergence condition on electric displacement) and the absence of free charge, $D(t)$ is uniform over the bar.

The simplest approximation of the bar's dynamics follows from the constant strain assumption and mass lumping. This is equivalent to a linear spring separating equal end masses $m = \rho AL/2$, as shown in Fig. 1. End displacements u_1 and u_2 are the degrees of freedom, whence governing equation (2.1) simplifies to the ordinary differential equations

$$m \frac{d^2 u_1}{dt^2} = F_{spr} + F_1 \quad , \quad m \frac{d^2 u_2}{dt^2} = -F_{spr} + F_2 \tag{2.3}$$

where F_{spr} is the spring force and F_1, F_2 are external forces applied at each end. Multiplying (2.2) by A and defining spring force $F_{spr} \equiv -AT$, electrode charge $Q \equiv AD$, spring compression $u \equiv u_1 - u_2 \equiv LS$, and voltage $V \equiv LE$ yields the piezoelectric spring constitutive relations

$$F_{spr} = -k^E u - d_m \dot{u} + \hat{e} V \quad , \quad Q = C^S V + \hat{e} u \tag{2.4}$$

$$k^E \equiv Ac^E / L \quad , \quad \hat{e} \equiv Ae / L \quad , \quad C^S \equiv A\varepsilon^S / L \tag{2.5}$$

where k^E, $\hat{e}$, and C^S are spring stiffness, piezoelectric force constant, and capacitance, respectively. Note that the spring equation is generalized above to include rate dependent mechanical damping through d_m. The sign convention on u is positive for compression and negative for extension. The spring idealization, governing equations, and constitutive relations are illustrated in Figure 1.

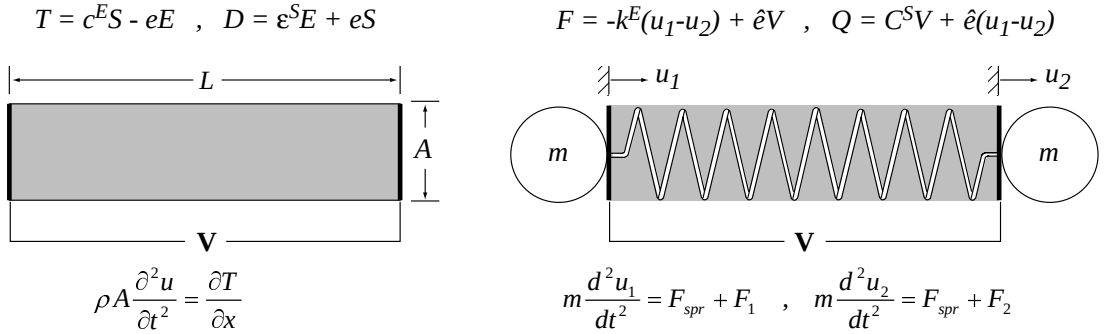

Fig. 1. Longitudinal piezoelectric oscillator (left) of length L and area A, and the equivalent simple harmonic oscillator model (right), showing the corresponding piezoelectric constitutive relations (above) and governing equations (below).

2.2. Simple harmonic oscillator solutions

Combining the spring-mass equations of motion and the spring constitutive relations yields two ordinary differential equations governing the piezoelectric oscillator. For example, consider the symmetric problem, i.e., $F_1 = -F_2 = F_{ext}$ and $u_1 = -u_2$, whence (2.3) and (2.4) yield

$$m\ddot{u}_1 + 2d_m \dot{u}_1 + 2k^E u_1 = \hat{e} V + F_{ext} \quad , \quad Q = C^S V + 2\hat{e} u_1 \tag{2.6}$$

Two canonical cases of interest are the "send" problem defined by voltage input and displacement output, and the "receive" problem defined by external force input and voltage output.

For the send problem, the differential equation and constitutive relation for current $i = d\dot{Q}/dt$ are

$$m\ddot{u}_1 + 2d_m\dot{u}_1 + 2k^E u_1 = \hat{e}V \quad , \quad i = C^S\dot{V} + 2\hat{e}\dot{u}_1 \tag{2.7}$$

When the prescribed voltage is time harmonic, $V(t) = V_0 e^{j\omega t}$, steady solutions are $u_1(t) = u_0 e^{j\omega t}$ and substituting gives

$$\frac{u_0}{V_0} = \frac{\hat{e}}{-m\omega^2 + j2d_m\omega + 2k^E} \tag{2.8}$$

Electromechanical response is given by the electrical impedance, i.e., voltage divided by current,

$$\frac{V}{i} = -\frac{j}{\omega}\frac{1}{C^S + 2\hat{e}u_0/V_0} \quad \left(= -\frac{j}{\omega}\frac{2k^E - m\omega^2}{C^S(2k^E - m\omega^2) + 2\hat{e}^2} \quad \text{for } d_m = 0 \right) \tag{2.9}$$

For the receive problem assume that current vanishes, hence, $Q = Q_0 = 0$ (without loss of generality, since Q_0 produces static compression and voltage that are removable by redefining equilibrium position and ground potential). The governing equation and constitutive relation for voltage become

$$m\ddot{u}_1 + 2d_m\dot{u}_1 + 2k^D u_1 = F_{ext} \quad , \quad C^S V + \hat{e}u_1 = 0 \tag{2.10}$$

where k^D is the stiffened spring constant

$$k^D \equiv k^E(1 + K^2) \quad , \quad K^2 \equiv \frac{\hat{e}^2}{k^E C^S} = \frac{e^2}{c^E \varepsilon^S} \tag{2.11}$$

and K is the piezoelectric coupling constant. For time harmonic external force, $F_{ext}(t) = F_0 e^{j\omega t}$, steady solutions are $u_1(t) = u_0 e^{j\omega t}$, $V(t) = V_0 e^{j\omega t}$ and substituting gives

$$\frac{u_0}{F_0} = \frac{1}{2k^D - m\omega^2 + j2d_m\omega} \quad \left(= \frac{1}{2k^D - m\omega^2} \quad \text{for } d_m = 0 \right) \tag{2.14}$$

Output sensitivity is defined as voltage divided by force,

$$\frac{V}{F_{ext}} = -\frac{2\hat{e}}{C^S}\frac{u_0}{F_0} \quad \left(= \frac{-2\hat{e}}{C^S(2k^D - m\omega^2)} \quad \text{for } d_m = 0 \right) \tag{2.15}$$

These simple, closed-form solutions exhibit most of the piezoelectric resonator characteristics that are of interest to the designer and modeler. Of course they are crude approximations despite being complete representations of 1D transducer physics. In contrast, more comprehensive models of the type described in this paper provide more complete, quantitative answers but without simple functional relations.

2.3. Coupled harmonic oscillator solutions

Generalizing the single piezoelectric oscillator described above to a coupled oscillator representing a transducer stack is straightforward and illustrated in Figure 2. The piezoelectric ceramic and matching layer(s) are replaced by piezoelectric or elastic springs with half of the mass lumped at each end. The water and backing loads are represented by dashpots with coefficient $d = I_m A$ where I_m is mechanical impedance of the load medium and A is cross-sectional area of the stack. This follows from 1D wave theory, which states that pressure p and velocity $\dot{x}$ are related as $p = -I_m\dot{x}$ where $I_m \equiv \rho c$ is the mechanical impedance of the medium.

Consider the single matching layer case. Coefficients and spring forces are

$$\begin{aligned} &m_1 = \tfrac{1}{2}L_1\rho_1 A_1 \quad , \quad m_2 = m_1 + m_3 \quad , \quad m_3 = \tfrac{1}{2}L_2\rho_2 A_2 \\ &d_b = \rho_b v_{Lb} A_1 \quad , \quad d_w = \rho_w v_{Lw} A_2 \\ &F_1 = -k_1^E(u_1 - u_2) + \hat{e}_1 V_1 \quad , \quad F_2 = -k_2(u_2 - u_3) \end{aligned} \tag{2.14}$$

where v_{Lb} and v_{Lw} are wave speeds (longitudinal) in the backing and water load. For simplicity we ignore intrinsic damping in the matching layer and piezoceramic. Equations of motion for the three masses are

$$
\begin{aligned}
m_1\ddot{u}_1 &= F_1 - d_b\dot{u}_1 = -k_1^E(u_1-u_2) + \hat{e}_1 V_1 - d_b\dot{u}_1 \\
m_2\ddot{u}_2 &= F_2 - F_1 = -k_2(u_2-u_3) + k_1^E(u_1-u_2) - \hat{e}_1 V \\
m_3\ddot{u}_3 &= -F_2 - d_w\dot{u}_3 = k_2(u_2-u_3) - d_w\dot{u}_3
\end{aligned}
\tag{2.15}
$$

The input is driving voltage $V = V_0 e^{j\omega t}$, hence, we seek the time-harmonic solutions

$$
u_1 = u_{01}e^{j\omega t} \quad , \quad u_2 = u_{02}e^{j\omega t} \quad , \quad u_3 = u_{03}e^{j\omega t} \tag{2.16}
$$

Substituting yields the symmetric, tri-diagonal system of equations

$$
\begin{pmatrix}
-m_1\omega^2 + k_1^E + j\omega d_b & -k_1^E & 0 \\
-k_1^E & -m_2\omega^2 + k_2 + k_1^E & -k_2 \\
0 & -k_2 & -m_3\omega^2 + k_2 + j\omega d_w
\end{pmatrix}
\begin{pmatrix} u_{01} \\ u_{02} \\ u_{03} \end{pmatrix}
= \hat{e}_1 V_0 \begin{pmatrix} 1 \\ -1 \\ 0 \end{pmatrix} \tag{2.17}
$$

This system of equations representing the forced vibration problem is easily solved as

$$
\frac{u_{02}}{V_0} = \frac{\hat{e}_1(m_1\omega^2 - j\omega d_b)(m_3\omega^2 - k_2 - j\omega d_w)}{\left\{\begin{array}{l}(m_1\omega^2 - k_1^E - j\omega d_b)(m_2\omega^2 - k_2 - k_1^E)(m_3\omega^2 - k_2 - j\omega d_w) - \\ k_2^2(m_1\omega^2 - k_1^E - j\omega d_b) - (k_1^E)^2(m_3\omega^2 - k_2 - j\omega d_w)\end{array}\right\}} \tag{2.18}
$$

$$
\frac{u_{01}}{V_0} = \frac{\hat{e}_1 + k_1^E \dfrac{u_2}{V_0}}{-m_1\omega^2 + k_1^E + j\omega d_b} \quad , \quad \frac{u_{03}}{V_0} = \frac{-k_2 \dfrac{u_2}{V_0}}{-m_3\omega^2 + k_2 + j\omega d_w} \tag{2.19}
$$

Intrinsic material damping in the piezoelectric and matching layer is included by letting

$$
k_1^E \to k_1^E + j\omega d_{m1} \quad , \quad k_2 \to k_2 + j\omega d_{m2} \tag{2.20}
$$

in these equations, where d_{m1} and d_{m2} are the mechanical spring damping coefficients.

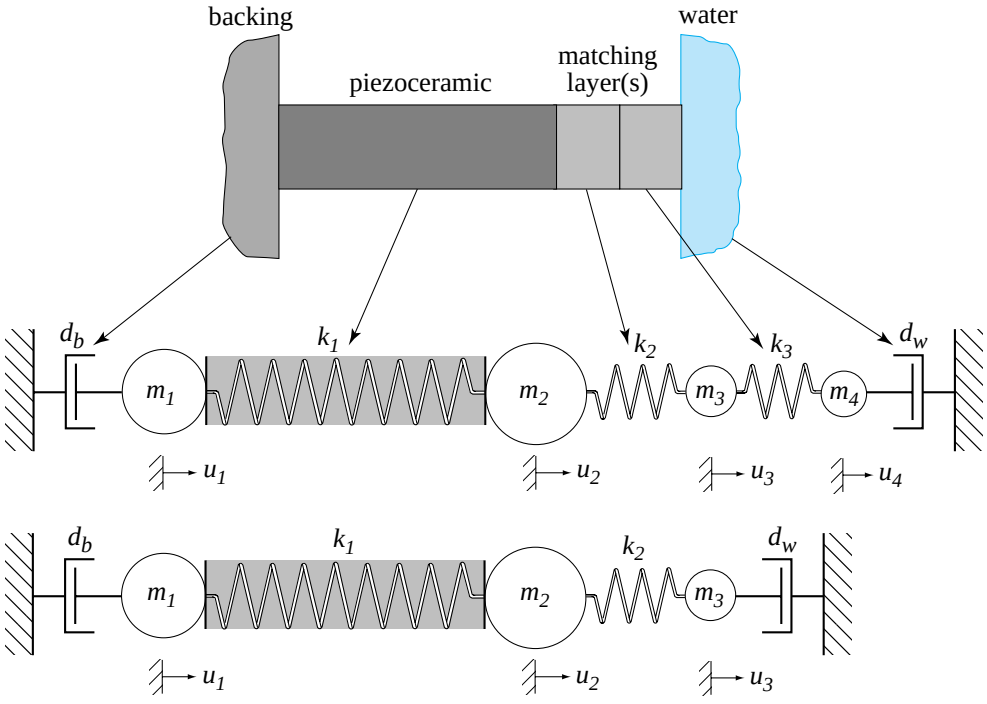

Fig. 2. Coupled harmonic oscillators representing the basic transducer stack with a single or double matching layer.

On this basis, closed-form solutions of coupled piezoelectric oscillator models are easily studied. They are the manifest, low order limit of representations ranging from electrical analogs like Mason and KLM models, to 1D wave propagation models, to broadband (transient) 2D and 3D finite element models. In terms of utility, such models have proven convenient as a "trivial" mathematical basis for demonstrating generic device behavior, and more specifically, for teaching fundamentals, illustrating matching layer design issues, and qualitative interpretations of transducer experiments and numerical simulations. More to the point, they are the archetype for 2D/3D finite element transducer models and an intuitive guide to proper electromechanical device modeling, particularly if the engineer's background has focused on electrical analog interpretations.

3. ALGORITHMIC FORMULATION OF PIEZOELECTRIC FINITE ELEMENTS

The concepts illustrated by the simple oscillator models above are generalized to full 3D behavior next, leading to the complete finite element formulation. This entails a dimensionality extension of course, but mainly raises the issue of effective computer-based solution schemes.

3.1. Governing differential equations (strong form)

Conventional polarized ferroelectric ceramics used in the manufacture of ultrasonic transducers are governed by the constitutive relations for linear piezoelectricity [13] and by the equations of mechanical and electrical balance. The electric balance is assumed instantaneous and decoupled, i.e., the quasi-static approximation of the electric field relative to the mechanical field. The governing equations are thus expressed:

$$\mathbf{T} = \mathbf{C}^E \cdot \mathbf{S} - \mathbf{e}^T \cdot \mathbf{E} \quad , \quad \mathbf{D} = \mathbf{e} \cdot \mathbf{S} + \boldsymbol{\varepsilon}^s \cdot \mathbf{E} \qquad \text{- constitutive equations-} \qquad (3.1)$$

$$\rho \ddot{\mathbf{u}} = \nabla \cdot \mathbf{T} \qquad \text{- momentum balance -} \qquad (3.2)$$

$$\nabla \cdot \mathbf{D} = 0 \qquad \text{- electric balance -} \qquad (3.3)$$

with $\mathbf{S} = \nabla^s \cdot \mathbf{u}$, $\mathbf{E} = -\nabla \phi$

where **T**, **S**, **E**, **D** are the mechanical stress, mechanical strain, electric field and electric displacement vectors, respectively. $\mathbf{C}^E$, $\boldsymbol{\varepsilon}^s$, **e** are the matrices of stiffness constants at constant electric field, of dielectric constants at constant strain, and of piezoelectric coupling constants, respectively. **u** is the mechanical displacement vector and $\ddot{\mathbf{u}} = \partial^2 \mathbf{u} / \partial t^2$ is the acceleration, each superposed dot "**.**" denoting one time differentiation. ϕ is the electric potential (voltage). To complete the description of the problem, equations (3.1)-(3.3) are complemented by appropriate boundary conditions, such as prescribed displacements or voltages, and applied forces or electric charge. These equations are the 3D counterparts to (2.1) and (2.2), with scalar quantities now replaced by matrices.

3.2. Semidiscrete finite element equations

The finite element method (FEM) is an approximation of the governing equations that is particularly well suited to computation. Whereas the differential form of the governing equations requires the solution to be exact at every point in space, the FEM is based on an equivalent variational or "weak" statement that enforces the "exactness" of the solution in a weighted average sense over small sub-regions of the space (the finite elements). For the class of formulations considered here, convergence and uniqueness of the solution can be established mathematically. In other words, error bounds on the approximation can always be determined and the approximation can always be improved such that the weighted error tends to zero at the limit, or equivalently, the finite element solution tends to the exact solution. In practice though, one does not require a zero error, but an error small enough to be insignificant compared to other sources of uncertainty (e.g., experimental errors in determining material properties, geometric dimensions, manufacturing tolerances), commonly lumped under the "umbrella" of noise.

The FEM requires the domain of the problem to be subdivided into small discrete finite elements: 4-node quadrilateral in 2D or 8-node hexahedron in 3D, for example. The solution sought is expressed in polynomial expansions with the coefficients of the polynomial being the value of the solution field at the finite element nodes. In other words, the FEM solution vector consists of the displacement values $\mathbf{u}_i$ and electric potential values ϕ_i at nodes i; the displacement and voltage fields at arbitrary locations within

elements are determined by a linear combination of polynomial interpolation (or shape) functions N_u and N_ϕ, respectively, and the nodal values of these fields as coefficients:

$$u(x,y,z,t) = \mathbf{N}_u(x,y,z).\mathbf{u}(t) = \mathbf{N}_u^e(x,y,z).\mathbf{u}^e(t) \tag{3.4a}$$

$$\phi(x,y,z,t) = \mathbf{N}_\phi(x,y,z).\Phi(t) = \mathbf{N}_\phi^e(x,y,z).\mathbf{\Phi}^\varepsilon(t) \tag{3.4b}$$

where superscript "*e*" denotes quantities associated with a given element. Equations (3.4) highlight key characteristics of the FEM as opposed to Rayleigh-Ritz methods, namely:

1) The nodal "unknowns" of the problem have physical significance (e.g., displacement) and are not just expansion coefficients.
2) FEM interpolation functions are local or element-based, implying the solution within an element is entirely determined by the solution at that element's nodes. It is this localization that permits element-by-element operations, and therefore allows the FEM to solve large-scale complex problems as an assembly of tractable, elemental contributions.

When the shape functions are taken to be linear, the strain distribution within the element is constant, just like the spring in Section 2. In that spirit, the quadrilateral/hexahedron continuum elements can be viewed as 2D/3D spring and mass combinations.

Incorporation of the spatial discretization (3.4) into the above mentioned variational statement results in a semidiscrete finite element system of linear algebraic equations, expressed in matrix form as follows:

$$\mathbf{M}_{uu}\ddot{\mathbf{u}} + \mathbf{C}_{uu}\dot{\mathbf{u}} + \mathbf{K}_{uu}\mathbf{u} + \mathbf{K}_{u\phi}\Phi = \mathbf{F} \tag{3.5a}$$

$$\mathbf{K}_{u\phi}^T\mathbf{u} + \mathbf{K}_{\phi\phi}\Phi = \mathbf{Q} \tag{3.5b}$$

where

$$\mathbf{M}_{uu} = \mathop{\mathbf{A}}_{e=1}^{nel} \int_{V_e} \rho \mathbf{N}_u^{eT}\mathbf{N}_u^e dV^e \qquad \text{- mechanical mass matrix -} \tag{3.6a}$$

$$\mathbf{K}_{uu} = \mathop{\mathbf{A}}_{e=1}^{nel} \int_{V_e} (\nabla\mathbf{N}_u^e)^T \mathbf{C}^E (\nabla\mathbf{N}_u^e) dV^e \qquad \text{- mechanical stiffness matrix -} \tag{3.6b}$$

$$\mathbf{K}_{u\phi} = \mathop{\mathbf{A}}_{e=1}^{nel} \int_{V_e} (\nabla\mathbf{N}_u^e)^T \mathbf{e}^T (\nabla\mathbf{N}_\phi^e) dV^e \qquad \text{- piezoelectric coupling matrix -} \tag{3.6c}$$

$$\mathbf{K}_{\phi\phi} = \mathop{\mathbf{A}}_{e=1}^{nel} \int_{V_e} (\nabla\mathbf{N}_\phi^e)^T \boldsymbol{\varepsilon}^s (\nabla\mathbf{N}_\phi^e) dV^e \qquad \text{- dielectric stiffness matrix -} \tag{3.6d}$$

$\mathbf{C}_{uu}$ is the mechanical damping matrix, **F** and **Q** are the nodal mechanical force and electric charge vectors, respectively, and **u** and Φ are the nodal displacement and potential vectors, respectively. The scheme by which elemental contributions are assembled to form the global system matrices is represented by the element assembly operator $\mathop{\mathbf{A}}_{e=1}^{nel}$. This element assembly process is akin to the simple one shown in (2.14), leading to (3.5) which is the 3D time-domain counterpart of (2.17).

Equation (3.5a) governs the mechanical or elastic portion of the problem, while equation (3.5b) describes the electrical field, and both are coupled through the piezoelectric coupling matrix. For passive materials, the coupling is null and equation (3.5a) fully describes the behavior of elastic materials. We note that inviscid and irrotational fluid (acoustic) media are sometimes more conveniently described by potential-based formulations [4,5], which we shall not describe here for the sake of brevity. Equations (3.5) are referred to as the semidiscrete FE equations in that space has been discretized whereas time is still represented as a continuous function. To solve such a system, assumptions and/or approximations on the time dimension must be made.

3.3. The time dimension and associated solution algorithms

Frequency-domain analysis: When the dynamic phenomenon is steady-state, with periodic forcing function and response at circular frequency $\omega = 2\pi f$, time dependence can be eliminated from the problem and the system unknowns convert to harmonic complex variables:

$$\mathbf{u} = \hat{\mathbf{u}}e^{j\omega t}, \qquad \mathbf{\Phi} = \hat{\mathbf{\Phi}}e^{j\omega t}, \qquad \partial(.)/\partial t = j\omega(.), \qquad \partial^2(.)/\partial t^2 = -\omega^2(.) \tag{3.7}$$

The FE equations (3.5) then reduce to a complex symmetric non-hermitian matrix system requiring an implicit solver. Direct implicit solution by Gaussian elimination is only practical in 2D because 3D leads to prohibitively large system bandwidth and memory needs. For larger problems, iterative solvers are indicated. For problems free of material and radiation damping, the system is positive definite and the conjugate gradient (CG) method is appropriate. In realistic situations though, various attenuation mechanisms (e.g., water loading) result in a typically indefinite system requiring more general iterative solvers such as GMRES [14] and QMR [15]. In practice, the utility of frequency-domain formulations diminishes as the phenomenon of interest involves multi-modal behavior, especially at higher frequencies. Even in transducers intended for steady-state operation, one typically analyses the spectrum around the narrow operational band to insure modal "purity", and that requires resolving the response over several discrete frequencies, with one full system solution for each. That is not to say that the utility of examining the data in the frequency-domain is diminished, since it is a concise and convenient visualization of complex behavior, but rather argues to the inefficiency of the algorithmic approach in such instances. In others words, the solution domain should be dictated by computational efficiency since the data can always be viewed in any desired domain through relatively speedy post-processing conversion by FFT. Many of the early FE implementations for piezoelectric dynamics were formulated in the frequency domain, most likely because of the early concentration on low-frequency sonar applications and the relative simplicity of extending real arithmetic elastostatic FEM to complex arithmetic harmonic elastodynamics FEM.

Eigenvalue/Eigenmode extraction: Classical eigenanalysis for extraction of natural frequencies and associated modal shapes also requires matrix factorization, whether direct or iterative, and these can be found in many textbooks. It should be noted though that eigenanalysis becomes computationally difficult as modal separation diminishes at higher resonances, and that the eigensolution only pertains to energy conserving (i.e., undamped) systems. Attenuation effects due to water loading or material damping are not accounted for. When damped modes are of interest, one needs to analyze the forced vibration problem (in either the frequency or time domain) for a range of the spectrum, identify resonances, and then extract the displacement field (i.e., mode shape) at these resonant frequencies.

Time-domain analysis: When transient or broadband signals are of principal interest, the temporal evolution of the system is best resolved through step-by-step time integration schemes. It is also the only solution approach if nonlinear phenomena are involved. There are many ways to determine the current solution at time t_{n+1} from known solutions at the previous time step t_n (algorithms involving higher order time approximations will involves several past time levels, but these tend to be reserved for special situations in view of the associated computational burden). The Newmark family of time integrators is widely used in mechanical dynamics. It assumes a constant acceleration $\mathbf{a} = \partial^2\mathbf{u}/\partial t^2$ over a small time interval (time-step) Δt and insures 2nd order accuracy in the temporal approximation. It takes on the following form when applied to the mechanical FE equation (3.5a):

$$\mathbf{v}_{n+1} = \mathbf{v}_n + \Delta t\left(\mathbf{a}_n + \mathbf{a}_{n+1}\right)/2$$

$$\mathbf{u}_{n+1} = \mathbf{u}_n + \Delta t\mathbf{v}_n + \Delta t^2\left[\left(1-\beta\right)\mathbf{a}_n + \beta\mathbf{a}_{n+1}\right]/2$$

$$\mathbf{a}_{n+1} = -\underbrace{\left[\mathbf{M}_{uu} + \frac{\Delta t}{2}\mathbf{C}_{uu} + \frac{\beta\Delta t^2}{2}\mathbf{K}_{uu}\right]^{-1}}_{\text{LHS}} \times \left[\overline{\mathbf{F}}_{n+1} + \mathbf{C}_{uu}\left(\mathbf{v}_n + \frac{\Delta t}{2}\mathbf{a}_n\right) + \mathbf{K}_{uu}\left(\mathbf{u}_n + \Delta t\mathbf{v}_n + \frac{\Delta t^2}{2}\left(1-\beta\right)\mathbf{a}_n\right)\right]$$

$$\overline{\mathbf{F}}_{n=1} = \mathbf{F}_{n+1} - \mathbf{K}_{u\phi}\,\boldsymbol{\Phi}_{n+1} \qquad (3.8)$$

Different choices of the Newmark parameter β result in temporal integrators optimized for different classes of problems:

Implicit methods (e.g., $\beta = 1/4$) couple current solution vectors, hence, the global system of equations must be solved at each time step. The LHS in (3.8) involves a matrix factorization (e.g., by Gaussian elimination) that is an expensive operation requiring a computational effort of order $O(n^2_{node}) \sim O(n^3_{node})$ and storage of order $O(n^2_{node})$. The advantage of implicit schemes is unconditional stability with respect to the time step. Implicit methods are typically indicated for statics (e.g., electrostatics (3.5b)), low-frequency mechanical or inertial dynamics, and diffusive processes (e.g., thermal diffusion) described by parabolic PDEs, where temporal gradients are substantially smaller than spatial ones.

Explicit methods decouple the current solution vectors and eliminate the global system solve, but they are only conditionally stable, i.e., there is a time step limit (CFL condition [16]) beyond which the algorithm becomes unstable. In elastodynamics, the CFL time step limit corresponds to the shortest transit time across any element in the mesh (Δt_{stab}=min(h/c), h is the element size or nodal distance, and c is the wavespeed). In wave phenomena, the desired resolution and accuracy require a time step smaller than one-tenth the period of the highest frequency of interest, a requirement no less stringent than that imposed by the CFL condition, and thus removing the principal advantage of implicit methods. It is this limit on the time step, and therefore on the distance traveled during each interval, that allows the nodal fields to decouple momentarily during a time step. Although not usually implemented in this fashion and for the purpose of this discussion, consider an explicit scheme as a Newmark integrator with $\beta = 0$ and $\mathbf{M}_{uu}$, $\mathbf{C}_{uu}$ diagonalized by nodal lumping. In this case, each equation in system (3.8) can be integrated independently, i.e., in a decoupled fashion. The coupling is then effectively accounted for through the forces on the right hand side of the equation, and these are vector operations that are much less demanding in computer resources than the matrix factorization required by implicit schemes. In actual implementation, the matrices shown in (3.8) are not assembled and stored, since an explicit scheme naturally structures itself into a series of element-by-element operations involving global vectors only. As such, storage and solution requirements scale linearly with the number of nodes in explicit schemes, which is still a requirement for useful 3D modeling. Element-by-element operations also offer a major advantage in code parallelization, which is gaining mainstream interest with the availability of multiple processor PCs.

The piezoelectric problem couples a mechanical dynamics process (3.5a) and an electrostatic one (3.5b). Computational efficiency would suggest that a mixed explicit/implicit scheme is optimal for the mechanical/electrical problem. This mixed scheme has been demonstrated to achieve a 2 orders of magnitude efficiency gain (computational speedup for a given model, or model size for a given computational time) with PZFlex [5] compared to conventional, fully implicit FEM implementations. This advantage is expected to be maintained as long as the electromechanical problem maintains a wave propagation characteristic, and increases markedly in large-scale applications. To illustrate the point, consider the naval flextensional transducer depicted in Fig. 3. This high power PMN-driven flextensional is one of 12 sources constituting a towed array, and the corresponding model requires about 10 million finite elements. An analysis of such large-scale and involving material nonlinearities (PMN) could only be undertaken today with an explicit scheme. Similar large-scale problems exist in the biomedical arena [10].

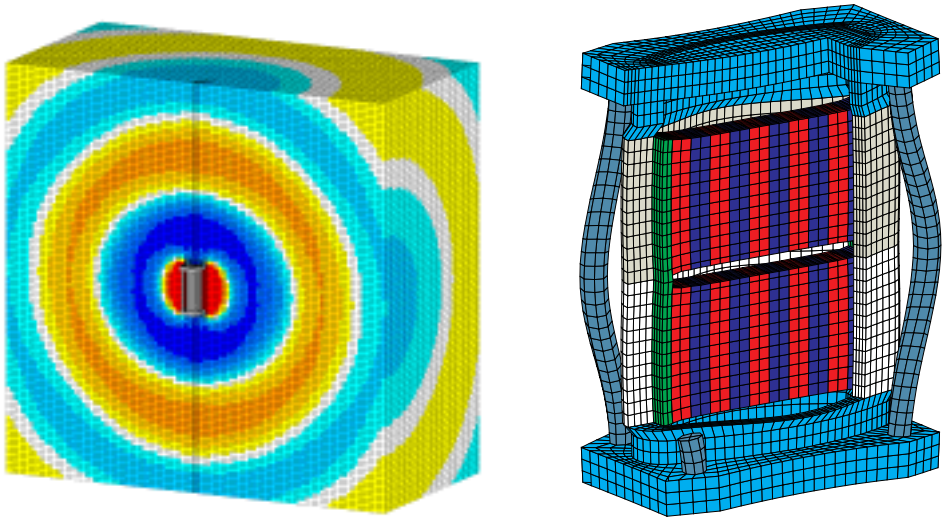

Fig. 3. Behavior of a single flextensional model driven in water, showing radiating wave pattern (left). View of mode shape in the single flextensional model driven at 4.5 kHz (right). A detailed description is available in [9]

4. FINITE ELEMENT MODELING ISSUES IN TRANSDUCERS AND ARRAYS

As in any analysis effort, the "quality" of the answers obtained depends not only on a good choice of methods but also on the input parameters used to define the model. Chief among these is material constitutive properties, which we discuss in detail in Section 5. Other parameters control the level of model fidelity to the physical behavior, typically optimized against computational cost. It is often argued that finite element simulation could be turned into a "black box" if computational resources were infinite. While this statement does point out a legitimate constraint, it ignores that one often has to analyze preliminary designs with tentative data and that different levels of approximations are appropriate for different questions. In what follows, we discuss some of the basic modeling issues underlying finite element simulation of transducers and arrays, and provide guidelines for the best use of these representations.

4.1. Spatial and temporal discretization

Meshing a finite element model defines the solution's resolution. For wave propagation problems, the discretization must resolve the shortest wavelength (i.e., highest frequency) of interest. This is analogous to crystal lattice theory [17] where the periodic discrete structure defines a low-pass filter with the highest frequency propagated (cutoff frequency) having a wavelength equal to 2h (h= finite element size or nodal distance); this is also known as the Nyquist limit or saw-tooth pattern. Obviously, one desires adequate rather than borderline resolution of the frequencies of interest, and this ranges from $\lambda/h = 8$ to 20 finite elements per wavelength. Discretization, by virtue of being on approximation process, introduces a numerical error that displays a non-physical frequency and direction dependent dispersive character. A wave pattern is well resolved with $\lambda/h = 10$ elements per wavelength (Fig. 4) and this produces a numerical dispersion error of about 3%. When long propagation distances are involved and wavefront or pulse distortions must be limited, gridding with 20 elements per wavelength limits the numerical error to less than 1% [18-20]. Because these frequencies propagate throughout the model, the same degree of discretization should be maintained throughout the mesh to avoid directionality and spurious internal reflectors. In practice, the finite element aspect ratio should remain close to one, but can safely reach 2 or 3 to accommodate geometric constraints. In contrast, a diffusive process such as heating tends to display localized spatial gradients and the degree of mesh refinement may vary from region to region accordingly (Fig. 4).

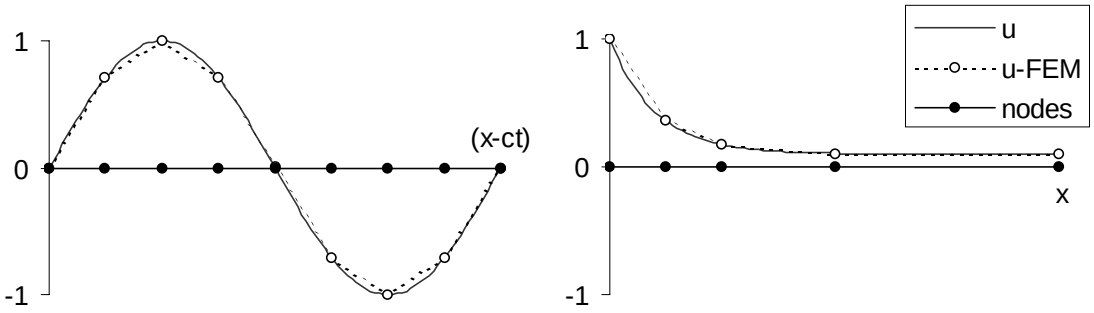

Fig. 4. Spatial discretization for wave propagation (left) vs. diffusion (right) problems.

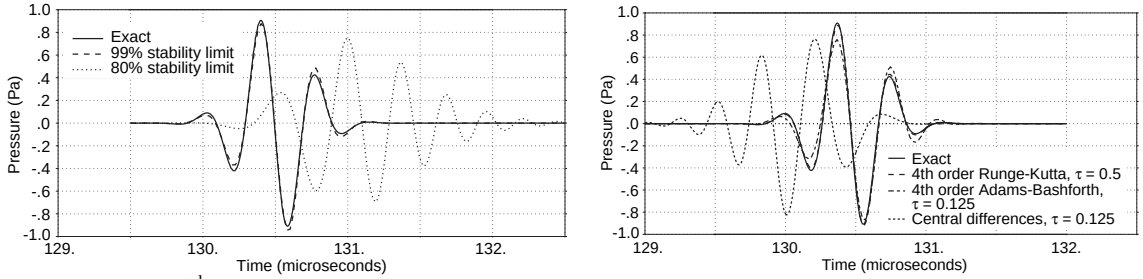

(a) In a 1D, 2nd order accurate grid (FE or FD).

(b) In a Pseudospectral grid integrated in time by leapfrog, Runge/Kutta, and Adams-Bashforth.

Fig. 5. Comparison of wavelet time histories after propagating 300 wavelengths [10].

Furthermore, because of the duality of space and time in the wave equation, the same criterion used for spatial discretization applies to time discretization, and means that the optimal time-step should be at the CFL stability limit. In practice though, only 90-95% of CFL in linear cases and 80% of CFL in nonlinear cases are achievable, which is sufficient for transducer analysis. However, when long-range wave propagation must be accurately described, in bioacoustic models for example, standard linear finite elements are no longer effective because of the accumulation of dispersion errors. Then, schemes such as the pseudospectral method using higher-order approximations must be used [10], as shown in Fig. 5.

Frequency content is not always the controlling factor in vibration problems. Geometric features and boundaries sometimes impose more stringent requirements on discretization. A prime example of this occurs in the case of the PZT half wavelength thickness resonator in a medical transducer stack. If discretization is set by wavelength considerations alone, the bar width would be divided into one or two finite elements across, which misses the lateral stress gradients due to Poisson effects. That lateral distribution influences coupling with an adjacent polymer matrix, for example, and gridding the width with 6 nodes is suggested if such effects need to be resolved.

4.2. Material Damping

Frequency-dependent material damping is an important issue in transducer modeling because of the many polymers involved including backing, matching layers, composite matrix, and lenses. Damping not only affects the acoustic signals but also generates heat. In the frequency-domain, the damping level can be specified at each discrete frequency, without concern as to overall frequency power laws and wide spectrum characterization. Classical time-domain finite element damping models are chosen for their operational and algorithmic properties rather than their phenomenological behavior. These models are restricted in their frequency dependence, but can vary from one element to another:

[a] Mass proportional damping yields an attenuation per unit distance that is constant with frequency, $\alpha = \alpha(f^0)$. The equivalent critical damping, which is a measure of attenuation per wavelength expressed as a percent of critical (level required for full attenuation over 1 wavelength), follows an inverse frequency dependence $\xi \propto 1/f$,
[b] Stiffness-proportional damping yields a quadratic dependence of attenuation $\alpha = \alpha(f^2)$ on frequency (critical damping $\xi \propto f$),
[c] Rayleigh damping allows for a linear combination of the mass and stiffness proportional models.
[d] Three-parameter viscoelastic models provide a slightly more complex behavior, with the attenuation exponent varying from 2 to 0 with increasing frequency, but are still amenable to FEM treatment.

These models provide an adequate fit, in general, over a range of frequencies as shown in Fig. 6. The Rayleigh damping model is versatile in that it provides a 2 parameter fit. Substantial improvement in matching experimental results is obtained when damping properties are specified independently for the volumetric (or longitudinal) and deviatoric (or shear) components, for most materials. Polymers and rubbers for example exhibit much greater attenuation of their shear components.

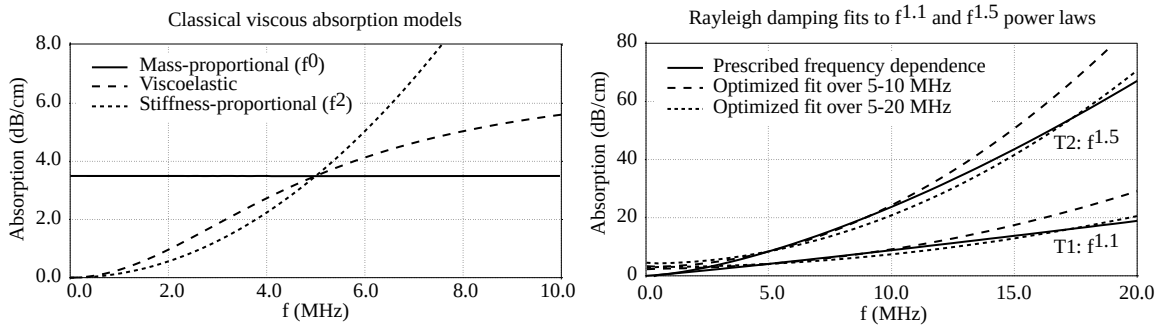

Fig. 6. Frequency dependence of various damping/attenuation models used in time domain wave propagation calculations (left), and Rayleigh damping fits to frequency power laws. All models are made to match a prescribed value at 5 MHz.

Viscoelastic models with more general frequency power laws can be formulated [21], but carry a high computational overhead because of the retarded integrals involved. Research into alternative forms amenable to explicit time-domain calculations [22] is ongoing and warrants further attention, but urgency on that front is tempered by the current limitations of experimental characterization of polymers.

4.3. Boundary conditions

It is often impractical to model the full extent of the transduction device and the surrounding acoustic media. In fact, considering that typical ultrasonic wavelengths are in the millimeter range at best, high resolution finite element simulations would be computationally exorbitant unless the domain was restricted to the area of interest. Truncation by an artificial boundary is required for domains large compared to the characteristic wavelength. Appropriate boundary conditions need to be imposed on the truncation boundary to simulate the behavior of a "continuing" medium. Waves incidents on the boundary need to exit the computational domain with no spurious reflections, consistent with the fact that the boundary is a mathematical construct and not an impedance mismatch zone (Fig. 7). Such boundary conditions have been termed radiation, transmitting, absorbing, non-reflecting or silent conditions. Reviews, extended reference lists, or comparative studies on this subject can be found in [23-25].

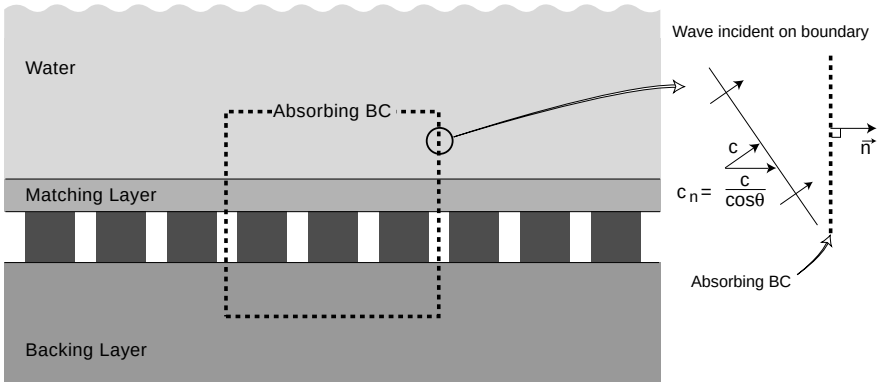

Fig. 7. Finite computational domain bounded by an artificial truncation boundary (dashed line) at which an absorbing boundary condition is applied.

There are no exact absorbing conditions applicable to all situations: frequency-domain, time-domain, nonlinear wave propagation. In the linear case, retarded potential integral formulations define an exact boundary condition, but one which is spatially and temporally non-local. Non-local schemes couple all degrees-of-freedom at the truncation boundary and all past time steps, which is impractical in realistic finite element studies because of their expense. Computationally attractive local schemes are based on varying degrees of approximation, with assumptions on the spatial decay rate of the radiating wave, its angle of incidence on the truncation boundary, and its wave speed. The common feature to all local radiation conditions is that they are asymptotically exact at high frequency, i.e., the wavelength is shorter than the scale of the boundary. The simplest and least accurate of these is the water load impedance condition, $p = -I_m \dot{x}$ where $I_m \equiv \rho c$ used in (2.14), which is exact in 1D but only asymptotically exact in the high-frequency/farfield limit in 2D/3D. The only currently available boundary treatment that is equally applicable to linear and nonlinear wave propagation is one recently proposed by Sandler [26] and implemented in PZFlex, for which we coin the acronym MINT (Material Independent Non-reflecting Treatment) condition. A brief derivation of the MINT condition is given below.

The normally propagating part on a wave traveling towards the truncation boundary is given by the Hadamard identity for outgoing waves $\partial/\partial n = (-1/c_n)\partial/\partial t$, where c_n is the unknown wave phase velocity in the direction of the outward normal n to the boundary. The Hadamard identity applies to the traction vector $\boldsymbol{\tau} = \mathbf{T}.\mathbf{n}$ at the boundary, $\Delta_n\boldsymbol{\tau}/\Delta n = -(1/c_n)(\Delta_t\boldsymbol{\tau}/\Delta t)$, so that the equation of motion or momentum balance yields a change in boundary nodal velocity:

$$\frac{\Delta_t \mathbf{v}}{\Delta t} = \frac{1}{\rho}\frac{\Delta_n \boldsymbol{\tau}}{\Delta n} = -\frac{1}{\rho c_n}\frac{\Delta_t \boldsymbol{\tau}}{\Delta t} \tag{4.1}$$

The Hadamard identity also applies to the boundary velocity field such that:

$$\frac{\Delta_n \mathbf{v}}{\Delta n} = -\frac{1}{c_n}\frac{\Delta_t \mathbf{v}}{\Delta t} \tag{4.2}$$

Combining (4.1) and (4.2) by eliminating the unknown wavespeed c_n yields the MINT condition:

$$\left(\Delta_t \mathbf{v}\right) = \sqrt{\frac{1}{\rho}\left(\Delta_t \tau\right)\cdot\left(\frac{\Delta_n \mathbf{v}}{\Delta n}\right)}\Delta t \tag{4.3}$$

This absorbing boundary condition makes no assumptions regarding material constitutive properties (i.e., nonlinearities can be accommodated), the boundary geometry, or angle of incidence of the scattered wave. The MINT condition has been shown to perform as well as a 4th order paraxial absorber [27], with lower computational overhead and less impact on stability.

Because of its unusual accuracy and its natural fit within a finite element approach, we should note the radiation boundary condition recently developed by Berenger, and coined the Perfectly Matched Layer or PML [28]. Although originally developed for electromagnetics, it has been shown to be applicable and particularly effective in acoustic wave propagation [10,29]. The PML construct is not universally applicable (e.g., nonlinear acoustics cannot be accommodated and the elastodynamic case has not been formulated to date), but it fills a crucial niche in the feasibility of large-scale bioacoustic models.

In practice, one needs to exercise some care in the placement of absorbing boundary conditions. They should be placed at some distance away from active sources where wave patterns are complex and gradients severe. This also avoids near grazing incidence on the boundary, where accuracy generally degrades. When cross-talk and coupling effects are of interest, the wave path must be kept in the computational domain, since a wave absorbed by the non-reflecting boundary condition cannot be reintroduced at another point. Finally, and when in doubt, a useful sanity check consists of plotting the pressure or stress waves patterns in the entire mesh and verifying that spurious reflections from the boundary are at second order error levels and not physically meaningful levels. In such circumstances, animations serve not only to explain complex interaction phenomena but also to validate the model.

Absorbing treatments are not the only boundary conditions that afford model reduction. Symmetry and periodicity concepts are equally crucial in effective solution approaches. Approximating finite spatial periodicity by an infinite periodicity is often used with the caveat that edge effects are filtered out. Similarly, reduction of a 3D structure with a "long" dimension to a 2D plane-strain model is also a routine modeling approach. Even when the aspect ratio does not justify such a reduction, a 2D analysis still serves the purpose of a "first cut" that can guide more exhaustive and expensive 3D studies. Examples in Section 6 and the listed references make evident the extensive and effective use of such reductions.

4.4. Farfield and nearfield extrapolation

Results at some distance away from the transducer are often of interest, such as beam patterns, at pulse-echo reflectors or focal points. Solution by finite elements would require field calculations in the intervening region between the source and the distant output points, which is of impractical. A better alternative is offered by exterior integral formulations that only require the discretization of a surface bounding the "source" region and only calculate the solution at specified output points. As such, they can be viewed as extrapolation methods. Integral formulations exist for propagation through homogeneous elastic media and even for multi-layered elastic media. In practice though, the simplest and probably most useful integral equations describe the radiation through homogeneous acoustic media (dilatational waves only), and we limit the discussion here to these instances.

<u>*Time-domain Kirchhoff integral equation*</u>: the exact expression for the time-dependent pressure at any point x_0 in the exterior infinite fluid surrounding the vibrating body (transducer), enclosed by a surface S, is given by the Kirchhoff integral equation:

$$p\left(x_0, t\right) = \int_0^t \iint_S \left[\rho \frac{\partial v_n\left(x_s, \tau\right)}{\partial t} G + \frac{\partial G}{\partial n} p\left(x_s, \tau\right)\right] dS \; d\tau \tag{4.4a}$$

with the Green's function G given by:

$$G = \frac{\delta(\tau - t + R/c)}{4\pi R} \text{ in 3D,} \qquad G = \frac{1}{2\pi\sqrt{(\tau - t + R/c)^2 - (R/c)^2}} \text{ in 2D} \tag{4.4b}$$

where R denotes the distance between the surface sampling points x_s and x_0, c is the fluid medium wavespeed. The pressure in the field is obtained from this convolution integral of pressure and normal acceleration $\partial v_n/\partial t$ time histories at the "sampling" surface. Since the Kirchhoff equation makes no approximations beyond the homogeneity of the surrounding unbounded acoustic medium, the solution is valid whether the field point is in the nearfield or farfield.

Although the integral theorem requires S to be a closed surface, often in practice we take it to be a plane surface on the front face of the model ignoring contributions from the other sides. This modeling approximation is reasonable to the extent that an effective aperture can be defined, but caution needs to be exercised when the model only represents a portion of the actual radiating device. The more substantial the sideway energy leakage (e.g., shear waves in matching layers) resulting in a larger aperture, the less valid is such a truncation. Another useful simplification in analysing medical arrays is to model the lens and surrounding water as one homogenous acoustic medium. Tthe surface data is then sampled at an intermediary level between the top of the matching layer and the absorbing boundary.

Frequency-domain farfield beam patterns: Beam patterns are by definition regarded as frequency-domain angular pressure distributions on a circle in the farfield. Although the Kirchhoff equation, or its frequency-domain counterpart known as the Helmholtz integral equation, could be used to calculate beam profiles, computational expense can be reduced by making use of the fact that $R \to \infty$. The governing integral equation reduces then to the Rayleigh-Sommerfeld diffraction equation

$$p_\infty(\omega,\theta) = \sqrt{\frac{k}{8\pi R}e^{i\pi/4}}\cos(\theta)\int_S e^{-ikR}\,p(x_s)dS \qquad \text{in 2D} \tag{4.5}$$

which can be further simplified with assumptions of ray acoustics and calculated efficiently using a spatial FFT [30]. Expressions similar to (4.5) also exist for the 3D case. Because of assumptions inherent in this formulation, the sampling surface is taken to be a plane, and concerns similar to those in the Kirchhoff case, regarding the definition and extent of the sampling surface, must be taken into account. Finally, it should be noted that the definition of a beam pattern, based on unimodal single frequency assumptions, does not always coincide with the beam experimentally obtained by sensing pulse (as opposed to CW) maxima along a circle in the farfield. They do coincide usually when the transducer response is dominated by a single well separated resonance.

4.5. Electric circuits

Ultrasonic transducers are invariably connected to some supporting electronics, frequently through a coaxial cable. During the design process, it is typically necessary to model the drive circuitry, the reception electronics and the intervening cable. When designing the electronics, it is most efficient to compute the impulse response of the transducer and use this in a circuit design code. When looking at the transducer details, it is more efficient to model the electronics directly. Fortunately, a few lumped parameter circuit elements (resistors, inductors, capacitors, and ideal transformers) usually suffice. Figure 8 shows generic drive (send) and receive circuits.

In the time domain approach, electrical boundary conditions on the electrodes are replaced by a coupled set of equations relating the voltage and charge (or their time derivatives) on the electrodes to the voltage and charge (or their time derivatives) throughout the circuit. The electrical boundary conditions (open, ground, applied voltage or current) then apply to the circuit rather than to the electrode. We note that the charges and potentials at each of the circuit elements are fully coupled to the nodal values throughout the FE model at each timestep. Careful algorithmic design is required to solve this system accurately and efficiently.

Electrodes themselves are typically modeled as voltage constraints, i.e., the voltage on each electrode node is constrained to be equipotential. This is almost always an accurate approximation, though windowing could be accounted for if need be and so can unusual electrical resistance. The mechanical effects of electrodes are typically neglected too. The electrode mass and stiffness could be accounted for, but they are usually negligible when compared to those of the ceramic.

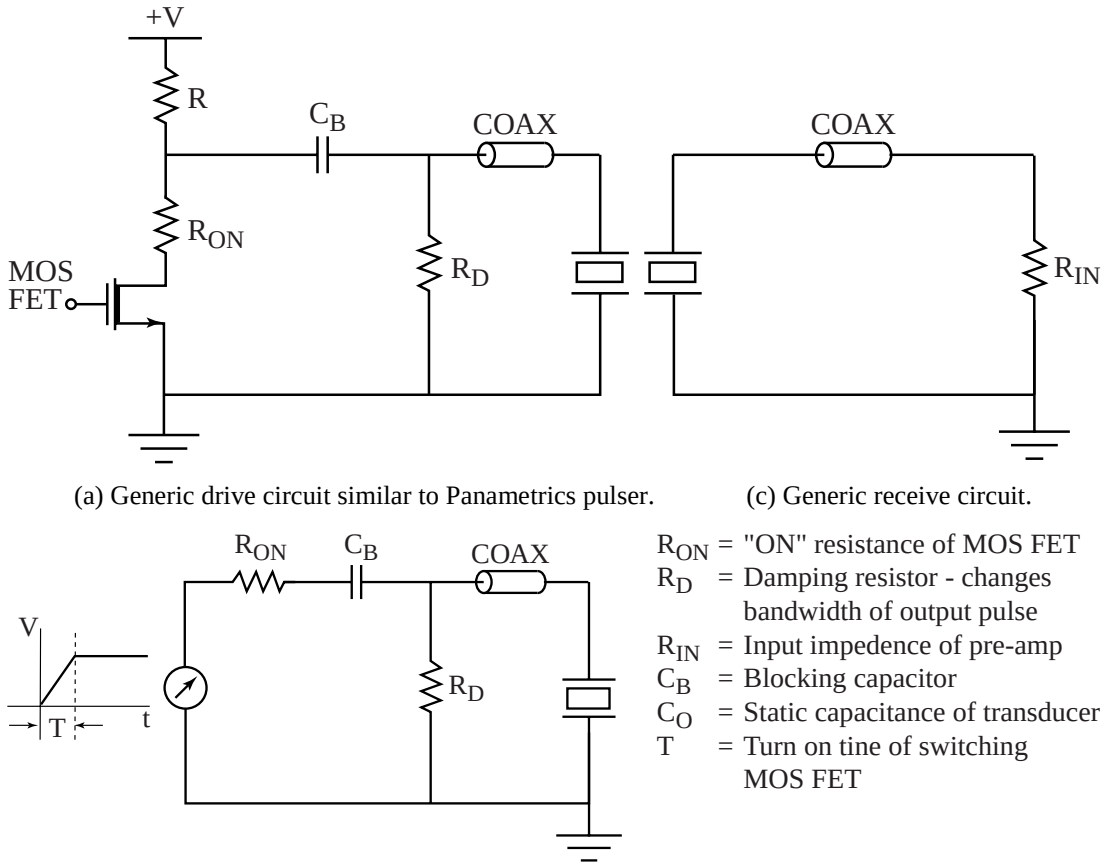

Fig. 8. Typical (a) send circuit, (b) its equivalent series circuit representation appropriate for incorporation in a finite element model, and (c) typical receive circuit.

5. MATERIAL CHARACTERIZATION AND INCREMENTAL VALIDATION

Before large-scale finite element models can be effectively utilized for the design of ultrasonic imaging systems, it is essential that these modeling tools be fully validated and key implementation issues identified. Furthermore, there is a need for a well-documented, nonproprietary "primer", that transducer designers can use to establish confidence in, and expertise with, the time-domain finite-element-modeling paradigm. The complete primer will consider issues such as material characterization, model configuration and model implementation (e.g. introduction of bondlines and electrodes).

The following sections describe a recent PZFlex validation exercise based around the incremental "*model-build-test*" analysis of a nonproprietary, 5MHz, 1D biomedical imaging array (Fig. 9). This type of incremental analysis permits transducer models to be developed that describe the transducer at each distinct stage of the manufacturing process. Consequently, deviations between experimental results and finite element predictions can be more readily analyzed and the transducer models refined as appropriate, i.e., sources of accumulative error are minimized.

5.1. Material Characterization

Accuracy of finite-element analysis is ultimately dependent upon the accuracy of the dielectric, piezoelectric and elastic properties used to represent the model's constituent materials. Consequently, in the course of this work, particular emphasis is placed on material characterization issues.

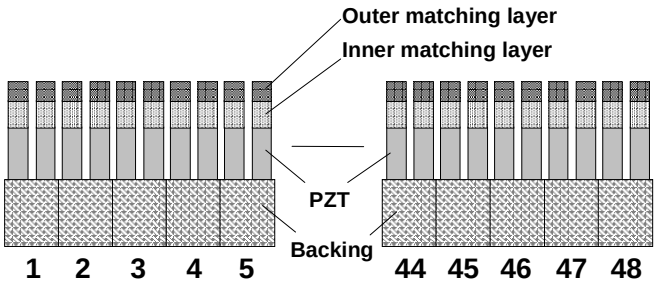

Fig. 9. Diagram of validation array assembly (2 PZT slivers per physical array element)

Piezoceramic properties are obtained via the application of curve-fitting techniques to IEEE standard resonator measurements [31]. The material properties are then cross-checked by comparing the experimental impedance responses for the IEEE standard resonators with the corresponding PZFlex predictions. In the work described here, matching layer and backing properties were obtained via a combination of through-transmission water tank measurements [32] and measurements made with a pair of contact shear-wave probes. Unfortunately, these measurement methods have several distinct drawbacks and hence, more comprehensive and accurate measurement schemes are currently being developed [33].

Piezoceramic Characterization: The IEEE standard on piezoelectricity [34] identifies certain geometrical shapes that may be used to facilitate the measurement of a material's elastic, dielectric and piezoelectric properties. For piezoelectric materials, there are 5 standard resonator geometries (Fig. 10). These resonator samples are specifically designed so as to isolate certain types of resonant behavior. Consequently, it is possible to measure those material properties that are strongly coupled to a particular resonant mode. The equations used to determine the material properties (as given in the IEEE piezoelectric standard [34]) have idealized derivations, and assume that the material is lossless. In practice, all real materials possess certain loss mechanisms, and hence the calculated properties will be subject to certain inaccuracies. A refinement to this method has been developed by researchers at the Royal Military College of Canada and employs curve-fitting techniques to more accurately determine a material's properties. The software package, PRAP [31], was used to perform this analysis and the extracted material properties for Motorola 3203HD PLZT are given in reference [35].

The IEEE resonators shown in Figure 10 were modeled in PZFlex using the measured properties given in [35]. Figures 11a-11d show the correlation between the experimental electrical impedance response and the corresponding PZFlex predictions for a selection of these resonator samples. In all cases, PZFlex is seen

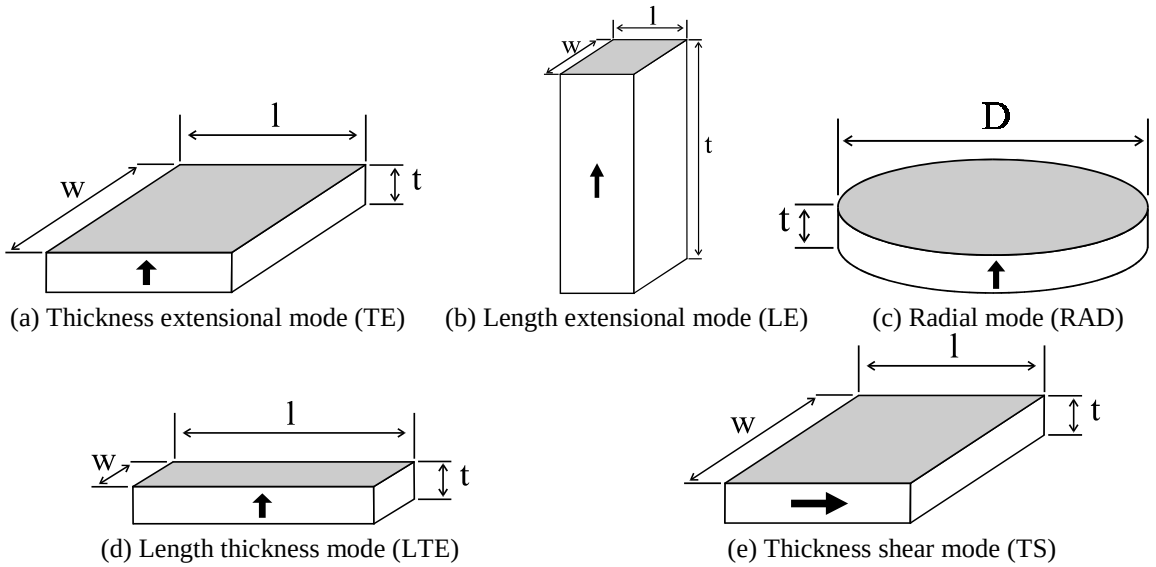

(a) Thickness extensional mode (TE) (b) Length extensional mode (LE) (c) Radial mode (RAD)

(d) Length thickness mode (LTE) (e) Thickness shear mode (TS)

Fig. 10. IEEE standard piezoelectric resonators:(a) TE, (b) LE, (c) RAD, (d) LTE, (e) TS.

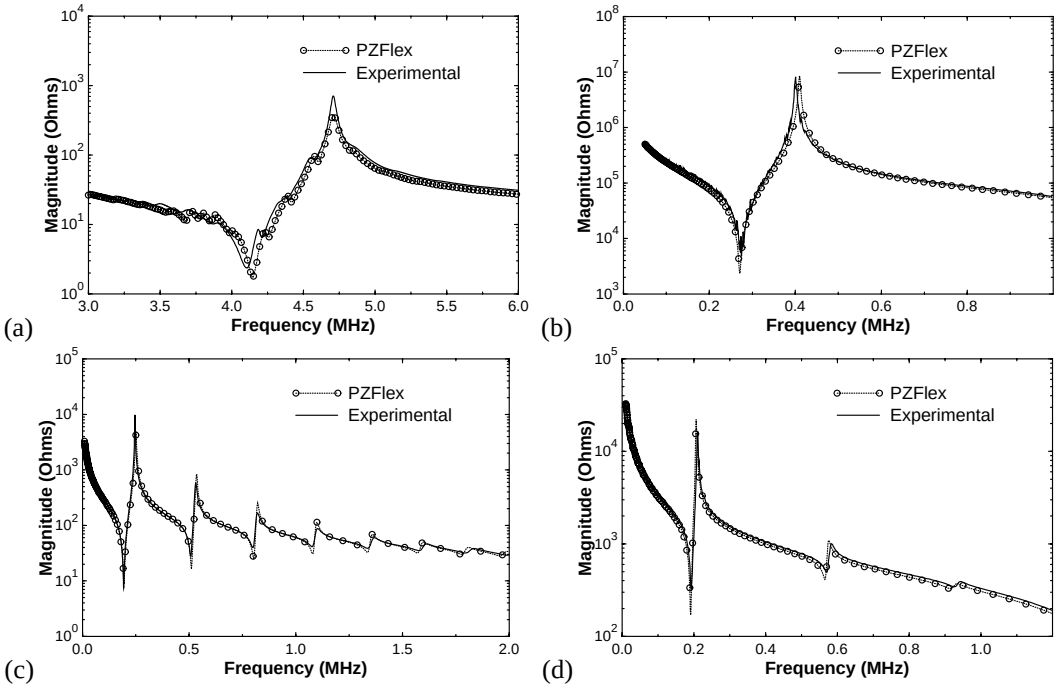

Fig. 11. Impedance magnitude response for resonators: (a) TE (upper left), (b) LE (upper right), (c) RAD (lower left), and (d) LTE (lower right).

to demonstrate excellent correlation with experimental results. The simulated in-air impedance response for the thickness extensional mode resonator (TE) correctly predicts the spurious modal activity lying between the electrical resonance at 4.1MHz and the mechanical resonance at 4.7MHz (Fig. 11a). These spurious resonances are due to lateral modes that are supported by the resonator's physical geometry. If these parasitic modes are too strongly coupled to the particular resonance of interest, the extracted material properties will be inaccurate. The TE resonator used in the current work effort was specifically chosen such that its dimensions fully satisfy the guidelines laid down in the IEEE piezoelectric standard. Since the other resonators have greater modal separation, their impedance response curves appear cleaner and more unimodal.

It is important to note that a given set of IEEE standard resonators will provide material properties that were measured over a range of different frequencies. For example, the TE resonator provides c_{33}^{D} at 4.7MHz whereas the LTE resonator yields d_{13} at 200kHz. Typically, all material properties will exhibit some degree of frequency dependence, however, with care, it is possible to select a set of properties that give consistent results over a wide range of frequencies.

Matching Layer and Backing Block Characterization: The validation array considered in this paper has a double matching layer and light acoustic backing attached to its upper and lower surfaces respectively (see Figure 9). Accurate characterization of these passive materials is just as important as for the piezoceramic. The material properties that need to be measured are longitudinal-wave velocity & attenuation, and shear-wave velocity & attenuation. Longitudinal velocity and attenuation measurements are relatively straightforward and may be accomplished via a simple through-transmission experiment. Unfortunately, measurement of the shear properties is typically much more difficult and potentially less accurate. Shear properties are normally obtained by attaching a pair of shear wave transducers to opposite sides of a test specimen and propagating a shear wave through the sample. Unfortunately, it often proves difficult to get good coupling of energy between the transducers and the sample. Consequently, the measured values are subject to considerable inaccuracies. Furthermore, these measurements are typically narrowband so results are only valid over a narrow range of frequencies. Wu at the University of Vermont is currently refining a wide-band, through-transmission, water tank characterization technique [33] for passive isotropic materials. It provides both velocity and attenuation data over a wide range of frequencies. Until material properties

obtained via this method become available, the characterization techniques described in [32] will be used to characterize the array's matching layer and backing block materials (see reference [35] for measured material properties).

5.2. PZFlex Validation – Incremental Array Samples

Once all the active and passive materials have been accurately characterized, it is feasible to proceed with PZFlex analysis of the transducer array assembly shown in Figure 9. This array is constructed from Motorola 3203HD PLZT and has 48 individual elements, each comprising two sub-elements as shown in Figure 9. A double layered, sub-diced matching layer was adopted and a "*light*" acoustic backing (Z≈2.5Mrayl) was bonded to the bottom of the device to help improve bandwidth characteristics while maintaining reasonable transmit sensitivity. For validation purposes, rather than attempting to model the entire array assembly, the analysis is currently restricted to the set of incremental array components shown in Figure 12(a). Each sample corresponds to half an individual array element, and was fabricated using the same techniques used to construct the complete array. Consequently, any process dependent effects should also be observed in the incremental samples.

The first step of the validation exercise is to confirm that the PZFlex prediction for each of these sub-units agrees with experimental values. Figure 12(b) shows both the experimental (——) and simulated (o·····o) electrical impedance response curves for Sample-1. At various stages throughout the fabrication process the piezoceramic slivers are subject to elevated temperatures and other process effects. These conditions cause the piezoceramic to partially depole, i.e. its piezoelectric coupling constants will be reduced. Consequently,

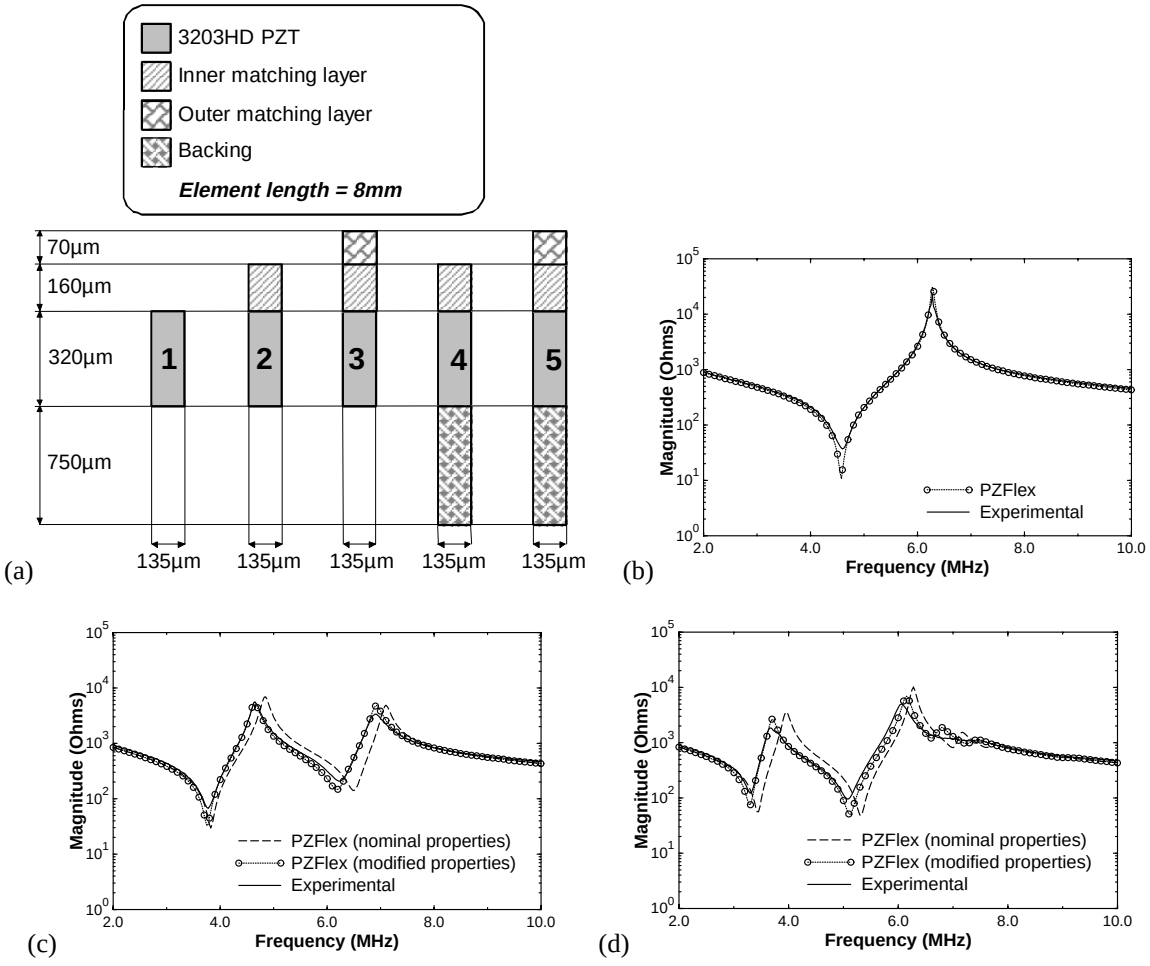

Fig. 12. (a) Diagram of incremental array components with sample numbers shown, and electrical impedance response for (b) Sample-1, (c) Sample-2, and (d) Sample-3.

5% depoling was assumed. From the cross-plotted results shown in Figure 12(b), excellent correlation between experiment and simulation are seen. Figure 12(c) shows the response for Sample-2 (single 320µm sliver of 3203HD with a 160µm inner matching layer). In this figure, the curve denoted (——) shows the experimental result, however, there are 2 simulated responses. The first curve, (-----), was obtained using the nominal matching layer properties given in reference [35], whereas the second simulated curve (o·····o) used velocities in the matching layer which were reduced by 10%. Furthermore, a 10µm bondline was also included in the calculation. Modified properties give much better correlation with experiment than the original nominal values. It was mentioned earlier that the matching layer properties are often difficult to measure accurately and that more accurate measurement methods are currently being developed. We expect to have more accurate material properties in the near future and anticipate that they will further improve the correlation with experiment. Sample-3 adds a 70µm outer matching layer to the Sample-2 configuration. The impedance characteristics for this device are shown in Figure 12(d) and the simulated result with bondlines and modified material properties is seen to compare well with the experimental result. It is interesting to observe that small changes in matching layer properties (longitudinal or shear) and the thickness of the bondline can have considerable impact on overall device response. This once again emphasizes the requirement for rigorous material characterization and accurate experimental measurements. Samples 4 & 5 correspond to the addition of the backing block to Samples 2 & 3 respectively (for impedance results refer to reference [35]).

6. APPLICATIONS: VISUALIZATION AND VIRTUAL PROTOTYPING

A picture is worth a thousand words, and a movie or animation of deformed shapes, pressure fields, electric fields, etc. is often worth much more. Practically speaking, model visualization is the ability to "see" the operation of a "virtual" device at convenient scales and speeds. It provides one of the most compelling reasons for numerical modeling. In addition to its technical merits, visualization, provide the best means of communicating concepts and designs to other engineers, customers, and management. This section describes some scenarios and applications illustrating the process.

6.1. Composites

Typically, preliminary transducer design is based on experience with similar devices, rules-of-thumb, and simplified 1D models. Once a preliminary design has been decided on, it is appropriate to build and run a finite element model. The computed impedance versus frequency curve will often reveal some unanticipated resonances that may affect device performance adversely. In this case, the next logical step is to compute and display or animate the deformation shapes at these resonances. Based on shape information and parameter studies, the designer is usually able to modify the design in order to minimize or eliminate the spurious modes.

A 1-3 composite transducer example from a matching layer study [8] is presented in Figures 13-15. The transducer is from an undersea imaging array designed by Ultrex Corp, built by Materials Systems Inc. and described in [36]. Fig. 13 shows measured and calculated impedance curves for the case of a water-loaded diced matching layer with filled and unfilled kerfs, while Fig. 14 shows deformation shapes at peaks on the beam pressure versus frequency plot for the filled case. The design frequency is 350 kHz. An unexpected mode is seen in Fig. 13 at 500 kHz for the case of air kerfs (left side). The extremes of deformation at this frequency are pictured in Fig. 15, showing a highly localized, matching layer mode. This is a lateral mode that couples strongly to bending modes of the PZT pillars in the 1-3 composite. Computer studies show that this mode disappears for a water load but if there is any shear stiffness in the load medium, as assumed in the calculation, e.g., an RTV lens, then this type of spurious mode can be supported.

Several finite element studies of composite transducers have appeared in the literature in the recent past, and good examples of 1-3 connectivity can be found in [3,37,38], and 2-2 connectivity in [39].

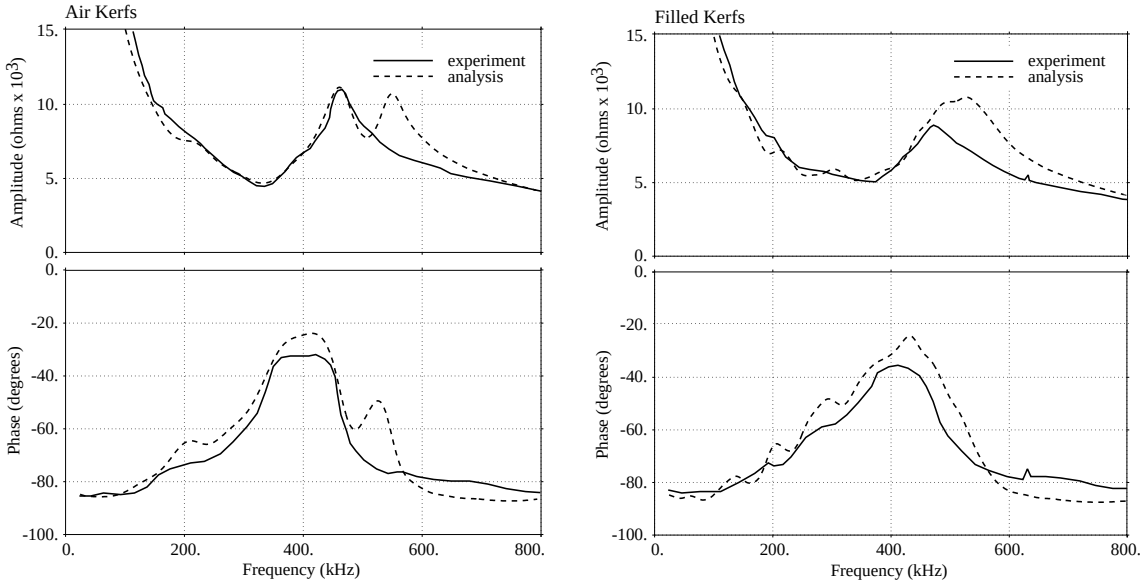

Fig. 13. Measured and simulated electrical impedance for the water-loaded MSI coupon, with and without matching layer kerf filler.

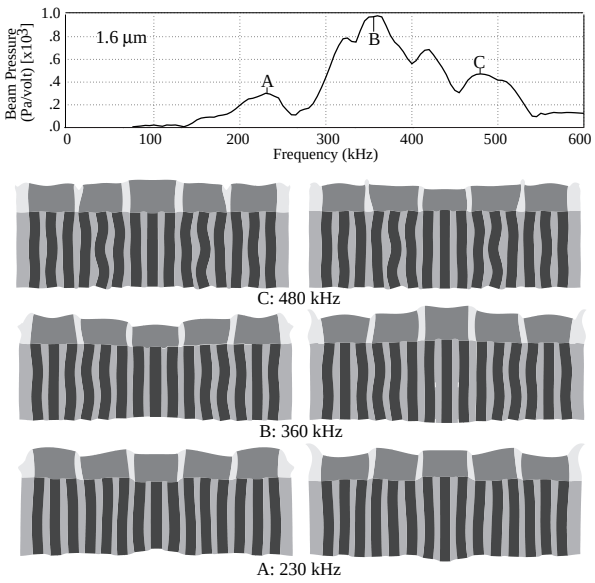

Fig. 14. Response charaterization of the composite model, showing detailed spectrum and mode shapes for the 1.6 mm thickness matching layer.

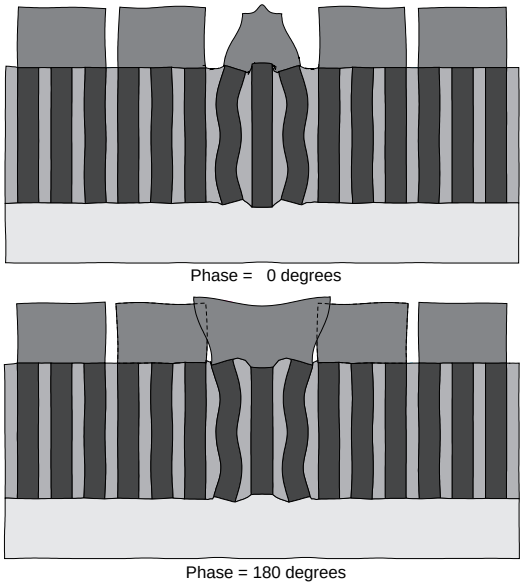

Fig. 15. Localized matching/pillar mode shapes at 500 kHz in Fig. 13 for air kerfs; calculated by a 3D model.

6.2. Therapeutics

Therapeutic ultrasound is another application where finite element modeling and visualization can be used to great advantage, both in transducer design and studies of ultrasound fields within the body. Here, the goal is to deliver a high intensity ultrasonic field to the target region while minimizing its effects on surrounding tissue. As an example, Figure 16 from [7] compares pressure fields from uniformly driven and phased transducer designs. In the latter case, phasing was used to move the focal region. Results were poor due to strong cross-talk between the continuous transducer rings.

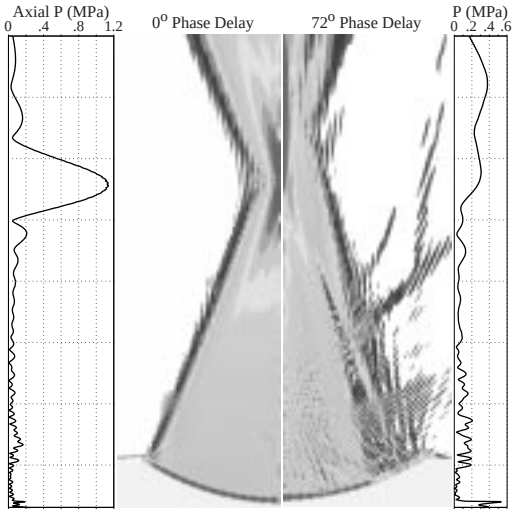

Fig. 16. Calculated field and on-axis pressure from a radially poled, 2 mm thick, PZT-5H spherical cap with 10 cm aperture and radius (f/1). Ten equal-area annular electrodes are driven by 1.0 volt at 1.0 MHz, uniformly (left) or phased (right).

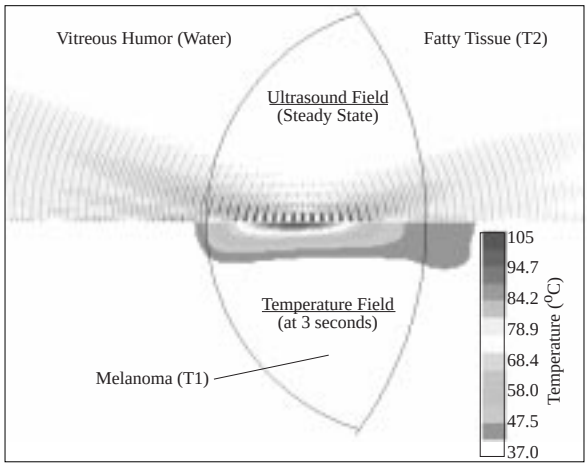

Fig. 17. Axisymmetric model of an ocular tumor, showing focused ultrasound beam (above) and temperature distribution at 3 sec (below). Note focal temperature in excess of 100 °C. The transducer has a 4 cm aperture and 9 cm focal length.

Because of high intensities at the focus, material nonlinearities in tissue become an issue. These include both compressive nonlinearity that is commonly described by the first nonlinear term (B/A) in an expansion of the pressure density relation, and cavitation under tensile stresses. Both of these are readily modeled in the time domain [7]. We note that material nonlinearity causes the generation of higher harmonics. Damping in tissue increases with increasing frequency, so these in turn induce greater losses and consequently higher heat generation. At extremely high intensities such as those found in lithotripsy, or at very long propagation distances, shock phenomena must also be modeled.

Transducer and wave field calculations are sometimes the means rather than the end of a simulation [7]. Figure 17 shows the computed pressure field (upper half) near the focus of a therapeutic ultrasound transducer. From this we calculate the thermal heat generation per unit time at each point in the model and then solve the bioheat equations for evolution of temperature with time. Temperature at 3 seconds is shown in the lower half of the figure. High temperatures can be used to destroy diseased tissue, but collateral damage to healthy tissue by thermal or cavitation mechanisms should be minimized. Simulations provide a convenient method to refine treatment strategies prior to in vivo validations on laboratory animals.

6.3 Prototyping

A last example is used to illustrate virtual prototyping of transducers. Fig. 18 shows a 3D model of a Tonpilz device for low frequency sensing in air. This classical design is usually used for water-loaded applications. The model consists of a tail-mass, a stack of four PZT rings, and a conical head-mass, all held together by a tension bolt through the axis. A thick matching layer with stiffening ring is bonded to the head mass.

One issue of interest for nominally axisymmetric devices is bending modes caused by nonsymmetric influences. One common influence is nonuniform driving by the piezoelectric rings. This was studied by introducing pseudorandom variation in the coupling constant around each ring. Both impedance and velocity spectra were examined to identify nonsymmetric modes. The principal bending mode was found at 7 kHz and shown on the left side of Fig. 18. The principal longitudinal mode was around 14 kHz, shown on the right side of Fig. 18. Higher harmonics of the bending mode were not apparent. Effects of mount locations and nonsymmetric mounting fixtures were also studied. Such analyses are readily done with numerical models and tend to reduce the need for an exhaustive set of prototype devices. Nonetheless, validation against experiment is mandatory.

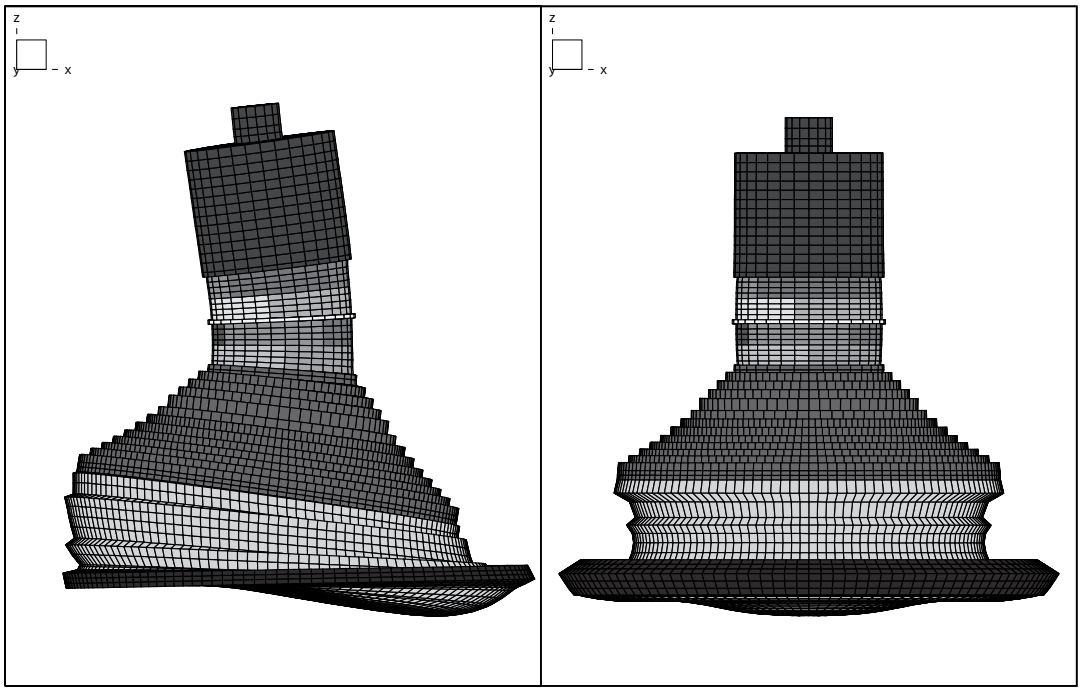

Fig. 18. Examples of bending (left) and longitudinal (right) modes of an air-coupled Tonpilz transducer. A thick, flexible matching layer is bonded to the face of the conical head-mass.

7. CONCLUSIONS

This paper was intended as a primer on various issues pertinent to finite element modeling of ultrasonic transducers. The breadth of the topic is vast and multi-disciplinary in nature, and this overview is perforce selective. We have attempted to review the basic algorithmic background and practical modeling issues to the extent they affect simulation strategies and capabilities. We have also tried to convey the idea that modeling is not an exercise independent of experimentation, whether to determine the requisite material properties or to develop intuitive understanding of the transducer's operational parameters. Much can be done to improve the accessibility of advanced simulation techniques, through intuitive graphical interfaces, standardized design "templates", and robust algorithms that require less interaction between the end-user and the "numerics". We do not foresee however that increased accessibility renders obsolete efforts to develop modeling skills and basic understanding of the underlying analytical methods. From our current perspective at least, these often effectively complement design skills: a good model reflects a good understanding of the physics.

8. ACKNOWLEDGEMENTS

This work was supported in parts under NSF SBIR Grant DMI-9313666, NIH SBIR Grant 1R43CA65255, and several ONR or DARPA/ONR contracts. We gratefully acknowledge the support and encouragement of our ONR monitors Dr. W.A. Smith and Mr. S. Littlefield. Various studies here mentioned were undertaken in collaboration with Dr. C. DeSilets of Ultrex Corp, Materials Systems Inc., Hewlett Packard, the Royal Military College of Canada, the Naval Undersea Warfare Center, UDI-Fugro Ltd., The Ultrasonics Group at the University of Strathclyde, the Riverside Research Institute and others, all of which we are grateful for.

9. REFERENCES

1. H. Allik and T.J.R. Hughes, "Finite element method for piezoelectric vibration", *Int. J. Num. Meth. Engng.*, Vol. 2(2), pp. 151-157, 1970.
2. H. Allik, K.M. Webman and J.T. Hunt, "Vibrational response of sonar transducers using piezoelectric finite elements", *J. Acoust. Soc. Am.*, Vol. 56, 1782-1792, 1074.
3. J.A. Hossack and G. Hayward, "Finite element analysis of 1-3 composite transducers", *IEEE Trans. Ultrason., Ferroelect., Freq. Contr.*, Vol. 38(6), pp 91, 1991.
4. R. Lerch, "Simulation of piezoelectric devices by two- and three-dimensional finite elements", *IEEE Trans. Sonics Ultrason.*, Vol. SU-37, 233-247, 1990.
5. G.L. Wojcik, D.K. Vaughan, N.N. Abboud and J. Mould, "Electromechanical modeling using Explicit-time-domain finite elements," *Proc. IEEE Ultrason. Symp.*, 2, 1107-1112, 1993.
6. G.L. Wojcik, D.K. Vaughan, V. Murray and J. Mould, "Time-domain modeling of composite arrays for underwater imaging," Proc. *IEEE Ultrason. Symp*., 1994.
7. G.L. Wojcik, J. Mould, F. Lizzy, N.N. Abboud, M. Ostromogilsky and D.K. Vaughan, "Nonlinear modeling of therapeutic ultrasound," *Proc. IEEE Ultrason. Symp*., 1617-1622, 1995.
8. G.L. Wojcik, C. DeSilets, L. Nikodym, D.K. Vaughan, N.N. Abboud and J. Mould, "Computer modeling of diced matching layers" *Proc. IEEE International Ultrason. Symp.*, 1996.
9. G.L. Wojcik, J. Mould, D. Tennant, R. Richards, H. Song, D.K. Vaughan, N.N. Abboud and D. Powell, "Studies of broadband PMN transducers based on nonlinear models" *Proc. IEEE International Ultrason. Symp*., 1997.
10. G.L. Wojcik, B. Fornberg, R. Waag, L. Carcione, J. Mould, L. Nikodym and T. Driscoll, "Pseudospectral methods for large-scale bioacoustic models" Proc. *IEEE International Ultrason. Symp.*, 1997.
11. N.N. Abboud, J. Mould, G.L. Wojcik, D.K. Vaughan, D. Powell, V. Murray and C. MacLean, "Thermal generation, diffusion and dissipation in 1-3 piezocomposite sonar transducers: finite Element analysis and experimental measurements" *Proc. IEEE International Ultrason. Symp*., 1997.
12. S. Przemieniecki, *Theory of Matrix Structural Analysis*, Dover Publications, Inc., 1968.
13. B.A. Auld, *Acoustic Fields and Waves in Solids*, Vol. 1, 2nd ed., Krieger Publishing Co., 1990.
14. R.H. Burkhart and D.P. Young, "GMRES acceleration and optimization codes", *ETA-TR-88*, Boeing Computer Services, May 1988.
15. R.W. Freund, "Conjugate gradient type methods for linear systems with complex symmetric coefficient matrices", *SIAM J. Sci. Stat. Comput*., Vol. 13(1), 1992.
16. R. Courant, K.O. Friedrichs, and H. Lewy, "Über die partiellen differenzengleichungen der mathematischen physik", *Math. Ann*., Vol. 100(32), 1928.
17. L. Brillouin, *Wave Propagation in Periodic Structures*, 2nd edition, Dover, 1953.
18. N.N. Abboud and P.M. Pinsky, "Finite element dispersion analysis for the three-dimensional second order scalar wave equation", *Int. J. Num. Meth. Engng*., Vol. 35(6), pp. 1183-1218, 1992
19. Z.P. Bazant and Z. Celep, "Spurious reflection of elastic waves in nonuniform meshes of constant and linear strain finite elements", *Comput. Struct*., Vol. 15(4), 451-459, 1982.
20. T. Belytschko and R. Mullen, "On dispersive properties of finite element solutions", in Miklowitz et al. (ed.), *Modern Problems in Elastic Wave Propagation*, pp. 67-82, Wiley, 1978.
21. T. L. Szabo, "Time domain wave equations for lossy media obeying a frequency power law", *J. Acoust. Soc. Am.*, Vol. 96(1), pp. 491-500, 1994.
22. M.G. Wismer and R. Ludwig, "An explicit numerical time domain formulation to simulate pulsed pressure waves in viscous fluids exhibiting arbitrary frequency power law attenuation", *IEEE Trans. UFFC*, Vol. 42(6), pp. 1040-1049, 1995.
23. D. Givoli, "Non-reflecting boundary conditions: a review", *J. Comp. Phys*., Vol. 94, pp. 1-29, 1991.
24. O.C. Zienkiewicz, P. Bettess, T.C. Chiam and C. Emson, "Numerical methods for unbounded field problems and a new infinite element formulation," in A.J. Kalinowski (ed.), *Computational Methods for infinite domain media-structure interaction*, AMD Vol. 46, pp. 115-148, ASME, 1981.
25. J.G. Blaschack and G.Z Kriegsmann, "A comparative study of absorbing boundary conditions", *J. Comp. Phys.*, Vol. 77(1), pp. 109-139, 1988.
26. I.S. Sandler, "A new procedure for wave propagation problems and a new procedure for non-reflecting boundaries", *Comp. Meth. Appl. Mech. Eng.* "special issue on exterior problems of wave propagation", accepted for publication, 1998.

27. R. Clayton and B. Enquist, "Aborbing boundary conditions for acoustic and elastic wave equations", *Bull. Seism. Soc. Am.*, Vol. 67, pp. 1529-1540, 1977.
28. J.-P. Berenger, "A perfectly matched layer for the absorption of electromagnetic waves", *J. Comp. Phys.*, Vol. 144, 185-200, 1994.
29. X. Yuan, D. Borup, J. Wiskin, M. Berggren, R. Eidens, S. Johnson, "Formulation and validation of Berenger's PML absorbing boundary for the FDTD simulation of acoustic scattering, *IEEE Trans. Ultrason., Ferroelect., Freq. Contr.*, Vol. 44(4), 816-822, 1997.
30. J. Bennett, *Development of a finite element modelling system for piezocomposite transducers*, Ph.D. dissertation, University of Strathclyde, Glasgow, Scotland, Nov. 1995.
31. PRAP – "Piezoelectric Resonance Analysis Program", TASI Technical Software, 174 Montreal Street, Kingston, Ontario, Canada, K7K 3G4
32. A.R. Selfridge, "Approximate material properties in isotropic materials", *IEEE Trans. On Sonics and Ultrasonics*, Vol. SU-32, No. 3, 1985
33. Junru Wu, "Determination of velocity and attenuation of shear waves using ultrasonic spectroscopy", *J. Acoust. Soc. Am.*, Vol. 99 (5), pp.2871-2875, 1996.
34. *IEEE Standard on Piezoelectricity*, The Institute of Electrical and Electronic Engineers, 1988
35. D. J. Powell, G.L. Wojcik, C.S. Desilets, T.R. Gururaja, K. Guggenberger, S. Sherrit and B.K. Mukherjee, "Incremental 'Model-Build-Test' Validation Exercise for a 1-D Biomedical Ultrasonic Imaging Array", *" Proc. IEEE International Ultrason. Symp*., 1997.
36. C. Desilets, *et al*., "Composite Curved Linear Array for Sonar Imaging: Construction, Testing, and Comparison to FEM Simulations," *Proc. IEEE International Ultrason. Symp.*, 1997.
37. G. Hayward, J. Bennett, and R. Hamilton, "A theoretical study of the influence of some constituent material properties on the behavior of 1-3 connectivity composite transducers", *J. Acoust. Soc. Am*., Vol. 98(4), pp 2187-2196, 1995.
38. G. Hayward and J. Bennett "Assessing the influence of pillar aspect ratio on the behavior of 1-3 connectivity composite transducers", *IEEE Trans. Ultrason., Ferroelect., Freq. Contr.*, Vol. 43(1), pp 98-108, 1996.
39. D.M. Mills and S.W. Smith, "Combining multi-layers and composites to increase SNR for medical ultrasound transducers", *Proc. IEEE International Ultrason. Symp*., 1997.